Myoglobin-Based Classification of Minced Meat Using Hyperspectral Imaging

Ayaz, Hamail

Multidisciplinary Digital Publishing Institute
2020-09-29

Ayaz, H.; Ahmad, M.; Sohaib, A.; Yasir, M.N.; Zaidan, M.A.; Ali, M.; Khan, M.H.; Saleem, Z. Myoglobin-Based Classification of Minced Meat Using Hyperspectral Imaging. Appl. Sci. 2020, 10, 6862.

http://hdl.handle.net/10138/348831

applied sciences

MDPI

Article

Myoglobin-Based Classification of Minced Meat Using Hyperspectral Imaging

Hamail Ayaz [1], Muhammad Ahmad [2,*], Ahmed Sohaib [1], Muhammad Naveed Yasir [1], Martha A. Zaidan [3,*], Mohsin Ali [1], Muhammad Hussain Khan [1] and Zainab Saleem [1]

1 Advance Image Processing Research Lab (AIPRL), Department of Computer Engineering, Khwaja Freed University of Engineering and Technology (KFUEIT), Rahim Yar Khan 64200, Pakistan; hamailayaz@gmail.com (H.A.); ahmed.sohaib@kfueit.edu.pk (A.S.); naveed.yasir@gmail.com (M.N.Y.); engineermohsinali@gmail.com (M.A.); hafiz.husain119@gmail.com (M.H.K.); zainab.saleem.370@gmail.com (Z.S.)

2 Department of Computer Science, National University of Computer and Emerging Sciences, Islamabad, Chiniot-Faisalabad Campus, Chiniot 35400, Pakistan; mahmad00@gmail.com

3 Institute for Atmospheric and Earth System Research (INAR)/Physics, University of Helsinki, FI-00560 Helsinki, Finland

* Correspondence: mahmad00@gmail.com (M.A.); martha.zaidan@helsinki.fi (M.A.Z.)

Received: 07 September 2020 ; Accepted: 25 September 2020 ; Published: 29 September 2020

Abstract: Minced meat substitution is one of the most common frauds which not only affects consumer health but impacts their lifestyles and religious customs as well. A number of methods have been proposed to overcome these frauds; however, these mostly rely on laboratory measures and are often subject to human error. Therefore, this study proposes novel hyperspectral imaging (400–1000 nm) based non-destructive *isos-bestic* myoglobin (Mb) spectral features for minced meat classification. A total of 60 minced meat spectral cubes were pre-processed using true-color image formulation to extract regions of interest, which were further normalized using the Savitzky–Golay filtering technique. The proposed pipeline outperformed several state-of-the-art methods by achieving an average accuracy of 88.88%.

Keywords: hyperspectral imaging; myoglobin (Mb) spectral features; *isos-bestic* points; substitution; Bovine (beef); Ovine (mutton); Poultry (chicken); minced meat; classification.

1. Introduction

Meat color is used to identify the different kinds of minced meat. Fresh meat that is protected from air contact (in vacuum packages, for instance) has a purple/red color which is the result of myoglobin's (Mb's) presence. Mb is one of the key pigments that are responsible for the color of meat. However, when the meat is exposed to air, Mb becomes oxy-Mb, which turns the meat a cherry red color [1]. In minced meat, the protein pigment, i.e., Mb, is generally categorized into three stages: dexo-myoglobin (DMb), meta-myoglobin (MMb) and oxy-myoglobin (OMb) [2]. Those states are used to classify meat color, type and age by assessing the oxidation using the Lambert–Beer law application [3–6].

The similarities in the Mb pigments of different species, as shown in Table 1, are used in the most common food fraud known as "substitution." Substitution fraud not only affects the consumer's lifestyle but also religious practices, diet and health [7]. In 2013, the selling of horse-meat brought a lot of attention to false labeling (substitution) issues in the meat industry [8]. Meat fraud is usually done due for financial benefit; e.g., mutton is two times more costly than beef [9]; therefore, selling beef in place of mutton will earn double the profit. Furthermore, meat fraud may cause serious health issues, such as allergies [10], gastric cancer [11], type-2 diabetes [12] and death [13]

in some extreme cases. To counter the substitution fraud, several classification techniques have been proposed, such as chromatography, drip loss, pH testing and DNA-based analysis [14–16]. However, these techniques require laboratory measures (manual operations) and are often subject to human errors [17–19].

Table 1. Similarity percentage among red meat and Poultry Mb [20].

Species	Beef	Buffalo	Sheep	Goat	Chicken
Beef	100				
Buffalo	98.0	100			
Sheep	98.7	96.7	100		
Goat	97.4	95.4	98.7	100	
Chicken	72.5	71.2	72.5	71.5	100

In addition to the traditional methods, multiple non-destructive imaging techniques (which only work in a visible spectrum, i.e., color, texture and marbling) have also been proposed [21–23]. These techniques deal with fresh, cold and stored meat through chemo-metric and regression based classification models, such as partial least square regression (PLSR), linear regression (LR) and support vector regression (SVR) [14,24,25]. However, imaging techniques (such as L*, a*, B*, chromatography and gray level co-variance matrix (GLCM)) only work with limited color information by utilizing only visible spectrum range. In advance to these traditional technologies, hyperspectral imaging (HSI) not only provides information about the spatial distribution but also the spectral information by examining a wide range of the electromagnetic spectrum.

HSI has been used in remote sensing [26–28], and the medical and food industries [29,30]. HSI is also being used for minced and whole meat-type classification [14,17,18,31,32]. For instance, Mahmoud Al-Sarayreh et al. [33] used HSI for adulteration detection of chunk meat types, i.e., mutton, beef and pork. These meat types were detected and classified using a support vector machine (SVM) and a convolutional neural network (CNN) with an accuracy of 94%. Furthermore, other meat properties, such as color, texture, marbling and exudation, were also examined [34–36], and they classified the pork meat as reddish pink (RFN), pale pinkish gray (PSE), pinkish firm (PFN), reddish soft (RSE) and dark purplish red (DFD). Qiao et al. [34] also exploited all those properties to classify the pork meat types using an artificial neural network (ANN) with an average accuracy of 78%–80%. Similarly, in 2017, Velas et al. [31] proposed a method to classify the 35 *longissimus dorsi* beef muscle samples depending upon their marbling patterns using HSI. To score the high classification rate, each muscle was examined through the decision tree (DT) classifier with 99.00% accuracy and 0.08% classification error. Barbon et al. [37] also used REPTree based on DT to identify and classify the chicken meat with 77.20% accuracy overall.

Minced meat classification has been examined by HSI-systems using regression-based models. For instance, Mohammed Kamruzzaman et al. [14] presented a study-based on V-NIR region to investigate the adulteration of horse meat in minced beef (Bovine) meat. The regression coefficients (R) were used to achieve the best calibration model with reduced dimensional data. The optimal PLSR model was established with coefficients of determination $R^2 = 0.99, 0.99, 0.98$ for calibration, cross-validation and prediction respectively. Ropodi et al. [25] proposed multispectral imaging-based detection of minced beef (Bovine) adulteration with horse minced meat using 110 samples of mince beef (Bovine) and horse. Adulteration identification was carried out using RF, PLSR-DA and SVM classifiers with an overall accuracy of 95.31%. Zhang et al. [38] used HSI-system in the V-NIR region to detect the adulteration of carrageenan in minced chicken meat by using absorbance (A) and Kubelka–Munck (KM) spectrums. Based on PLSR classification results, absorbance spectra were found to perform best with a Root Mean Square Error of Prediction Set (RMSEP) of 0.48 and a coefficient of determination for prediction data (R_p^2) of 0.92. Similarly, Rady et al. [39] proposed the effectiveness of hyperspectral imaging (400 × 1000 nm) for minced meat adulteration using three adulterants textured vegetable

protein (TVP, beef and pork). The adulteration was estimated using a PLSR model to achieve a ratio between performance and deviation (RPD) of 0.69 for beef adulteration with pork and 0.93 for beef adulteration with TVP.

The aforementioned studies only used classical patterns of HSI, which affects the reliability of adulteration detection systems, as these highly depend upon the meat marbling and texture patterns. Moreover, they requires homogeneous samples which are subjected and hard to reproduce methods; e.g., a sample with inter-muscular fat can not be measured correctly if the system has been trained on a different texture pattern. This study presents two novel contributions. First, as per the author's knowledge, for the very first time we have formulated a true-color image of HSI data to correctly segment the meat images. Second, this study proposed a (*isos-bestic*) Mb-based spectral feature classification method for minced meat to help in eradicating the substitution fraud from the meat industry.

2. Materials and Methods

This section describes the sample preparation, data acquisition, pre-processing, image correction and segmentation. The key steps of the methodology are listed below:

1. **Meat sampling:** Purchasing and mincing of Bovine/beef, Ovine/mutton and Poultry/chicken. To ensure no adulteration in minced meat types, proper cleaning of mixer is done every time, prior the mincing process.
2. **HSI-sytem:** Data acquisition using HSI system and calculation of reflectance and absorption.
3. **Pre-processing:** Formation of a true-color image to select the exact region of interest (ROI).
4. **Spectral features:** Extraction of intensity features through spectral characteristics of the *isos-bestic* point of Mb pigments.
5. **Classification:** Classification of minced meat types using SVM.

2.1. Meat Sampling

In total, 60 samples (20 Bovine/beef, 20 Ovine/mutton and 20 Poultry/chicken) were acquired in 35 days in the months of November and December from a commercial abattoir in the of city Rahim Yar Khan, Pakistan, within 1 hour of slaughtering. The meat chunks were sealed in a zip-locker plastic bag and placed in an ice cooler box (0–4 deg C) to ensure the freshness of the meat. The meat was transported to the laboratory within 1 h of sample collection. Furthermore, to ensure equal volume and weight of each meat type, the gathered samples were minced using an electronic mincer with two cross blades for approx 5–7 s. During the mincing process, the mixer was properly cleansed after mincing each meat type. Finally, the minced meat was placed in the cylindrical container for data acquisition. The samples were measured using an HSI system after approximately 15 min intervals post-mincing. On the average, the complete data acquisition of each sample was done 2 h and 30 min postmortem. Moreover, in order to ensure that the Mb pigments' values remained intact in fresh meat, it was important to perform the procedure in 2–4 h, or else the Mb pigments would have deteriorated to form a darker brown color due to the longer exposure to oxygen [2].

2.2. Data Acquisition

A push broom/line scanner HSI system (Specim Fx 10) was used in this study. The laboratory setup is shown in Figure 1a. This scanner was coupled with a 1.4/8 mm lens having a numerical aperture of 1.7 and can capture the effective pixel size of 19.9×9.97 µm with the spectral sampling of 2.7 nm. HSI system was also coupled with a flat moving translational stage having a size of 21×40 cm. The system captures the visible and near infra-red (V-NIR) range of electromagnetic spectrum (395–1000 nm). The other components attached to HSI system were 3 halogen lamps of 75 Watt light capacity and color temperature of 3350 kelvin and a laptop supported by data capturing

software (LUMO scanner) using a serial communication port via pleora *GigE–Vision* connector. Finally, to ensure the removal of ambient noise, the whole system was kept in a dark box.

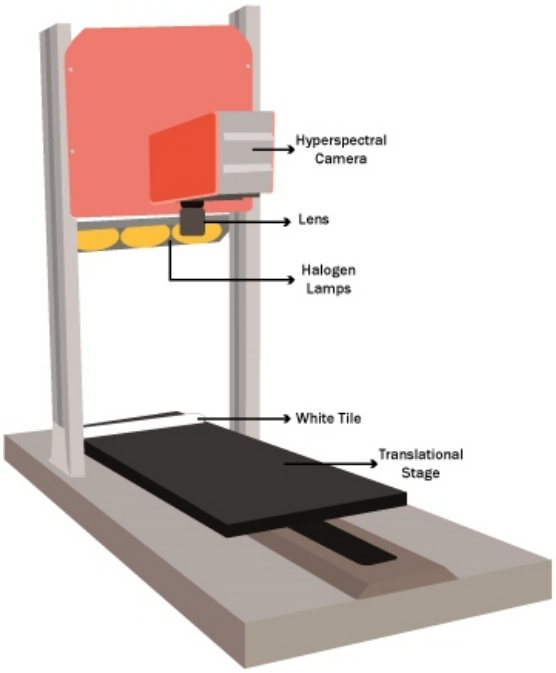

(**a**) V-NIR Hyperspectral Imaging System.

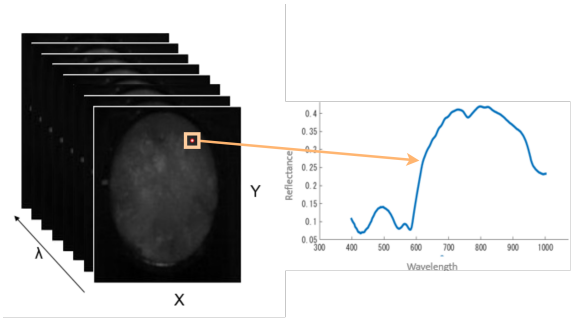

(**b**) Spatial and Spectral information of Beef Class.

Figure 1. Laboratory protocol (Specim Fx 10) used in this study for minced meat data acquisition.

To ensure equal quantity for each sample, a glass cylindrical container was used to contain 65 g of minced meat. During data acquisition the spatial binning was set as 2 × 2. The frame rate was set as 60 fps while the exposure time was 16 ms. The translational stage moved with the speed of 25 mm/s which captured the composition of sample using row by row operation. The stage also had a *ceramic* white reference tile fixed at the start position of the translational medium and captured 100 rows for each sample. In addition, 100 rows of dark frame were also captured by using the closing of camera's shutter.

Image Correction

The HSI system used in this study acquired 224 spectral bands (λ) with 789 × 512 spatial pixels due to the acquisition software (Lumo Scanner), as shown in Figure 1b. The spectral radiance cube generated by the HSI system includes the sensor's noise, illumination and several other atmospheric effects (air particles, light effects, particle size, etc.), which can cause false results [40]. Therefore, to exclude those effects, actual reflectance of the object was calculated by using the imperial line method [41]. For reflectance calculation a dark and white reference is required to remove the atmospheric effects. Thus, white reference W was captured by scanning a white tile and the dark reference b was captured by obscuring the camera lens fully using an opaque black cap. All the samples were prepared in the same way using Equation (1).

$$R = \frac{Rad - b}{W - b} \tag{1}$$

where R is the normalized accurate reflectance cube; Rad represents spectral radicance captured by HSI-system, with 0% reflectance for b and 99.9% for W. Furthermore, each minced meat spectrum absorbs some portion of light, which cannot be observed through normal visualization [2,42]. Therefore, the absorption values of minced meat were computed by using Equation (2) [14,43];

$$A = \log \frac{1}{R} \tag{2}$$

where A and R represent absorption and accurate reflectance cube, respectively. The calculated absorption spectrum represents the composition of chemical bonds; for instance, the 430 nm wavelength band contains information about absorption of hemoglobin pigments, the 500–600 nm one about respiratory pigments and 760 nm, 940 nm and 996 nm about the second overtone of O–H [32,44] in the minced meat spectrum.

2.3. Spatail-Spectral Pre-Processing

2.3.1. Spatial Pre-Processing

Generally, an HSI cube contains a rich amount of information, which is computationally complex. Therefore, the region of interest (ROI) needs to be extracted, and usually, in HSI systems a random image is selected from all bands for this purpose [14,18]. The selected image needs further image processing, for instance, image adjustment, binary thresholding or morphological operations, to extract ROI. Furthermore, the selected random band image may contain some extra information regarding some components of sample like muscular fat which can effect the segmentation. Therefore, the true-color image of each sample was formed for further processing.

True-Color Image:

To compute the true-color image, each visual region of accurate reflectance cube was divided into three sub-regions, θ_R, θ_G and θ_B with the segmentation wavelength ranges: R, 610–700 nm; G, 500–570 nm; and B, 450–500 nm [45]. Thus, for each segmented region, the correlation coefficient $\rho(X,\ Y)$ was computed by Equation (3).

$$\rho(X, Y) = \frac{C(X, Y)}{\sigma_X \sigma_Y} \tag{3}$$

where ρ represents the correlation coefficient of X, Y and σ_X; and σ_Y represents the standard deviation of X and Y. The co-variance matrix C was computed by Equation (4) [46].

$$C(X, Y) = \frac{1}{N} \sum_{i=1}^{N} (X_i - \mu_X)(Y_i - \mu_Y) \tag{4}$$

where μ_X and μ_Y represent means of X and Y. The correlation coefficient returns a value in the range of $(-1, 1)$—anti-correlation at -1 and high correlation at 1. The sum of the three highest average correlations, within the segmented regions, were coupled to produce a true-color image, as shown in Figure 2. Moreover, Figure 2a–c shows the true-color images of Bovine, Ovine and Poultry minced meat, which were reduced to the size of 159×165 for better visualization and understanding of the reader and contain background of both the tray and the glass cylinder edges. Furthermore, other methods use an illuminant to compute true-color images, such as CIE-D65 and CIE-D50 [2,17].

Finally, blob analysis technique was used to extract ROIs of each sample from true-color image, which analyzed the minced meat through color values, surrounding regions and brightness level. The detail color information of true-color image produced very precise and accurate ROIs as shown in Figure 2. The size of extracted ROI for each sample was $60 \times 50 \times 224$ and is shown in Figure 2d–f.

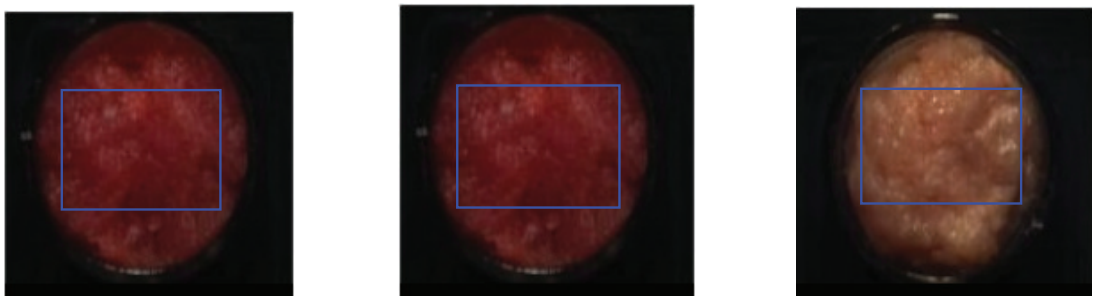

(**a**) Bovine true-color image (**b**) Ovine true-color image (**c**) Poultry true-color image

(**d**) Bovine true-color image ROI (**e**) Ovine true-color image ROI (**f**) Poultry true-color image ROI

Figure 2. True-color images generated using correlation coefficient method and the generated ROIs. (**a**) Bovine minced meat; (**b**) Ovine minced meat; (**c**) Poultry minced meat; (**d**) Bovine ROI representation; (**e**) Ovine ROI representation; (**f**) Poultry ROI representation.

2.3.2. Spectral Pre-Processing

The segmented regions needs to be pre-processed due to highly sensitive natural properties of light which generate random noises (size, shape and distribution of particles [47]) in the minced meat spectrum. Therefore, to eliminate these noises, Savitzky–Golay Filtering [48] is applied to the segmented region as a spectral pre-processing method. Golay filtering works by applying polynomial fitting to the input spectrum and preserve the spectral features rather than eliminating noise; i.e., low filtering can result in spectral noises and too much filtering can flatten the spectral response, which can alter the effects of classification. The effect of spectral smoothing can be seen in Figure 3.

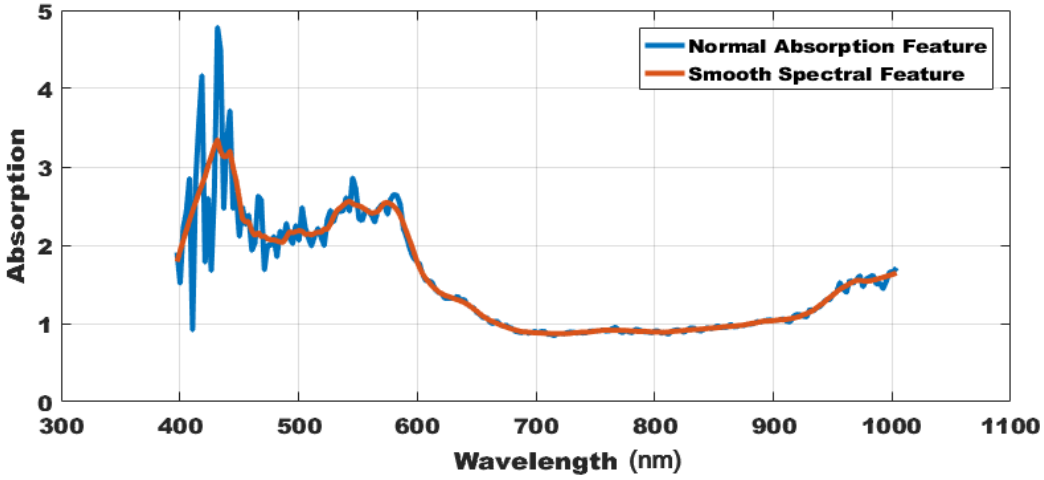

Figure 3. Comparison between pre-processed spectrum (Smoothing spectrum) and computed spectrum (normal spectrum) of Bovine minced meat.

2.4. Spectral Features

After noise removal, the feature extraction process is carried out based on the Mb pigments found in the minced meat class. MetaMb (MMb), DexoMb (DMb) and OxyMb (OMb) represent protein

pigments which have a spectral intersection at wavelength of 525 nm [2]. This intersection point is known as the *isos-bestic* point of Mb pigment. This *isos-bestic* point in Mb pigments can be utilized to extract the spectral features for minced meat classification. The mathematical representation of *isos-bestic* feature extraction is found in Equation (5):

$$F_i = \frac{A_\lambda}{A_{49}} \tag{5}$$

where λ represents wavelength bands which are 224 in this study, the 49 band represents the wavelength of 525 nm, A represents the absorption and F_i is the proposed feature extracted at wavelength λ. The sample spectral features for Bovine, Ovine and Poultry are shown in Figure 4. These spectral features are further utilized for model training.

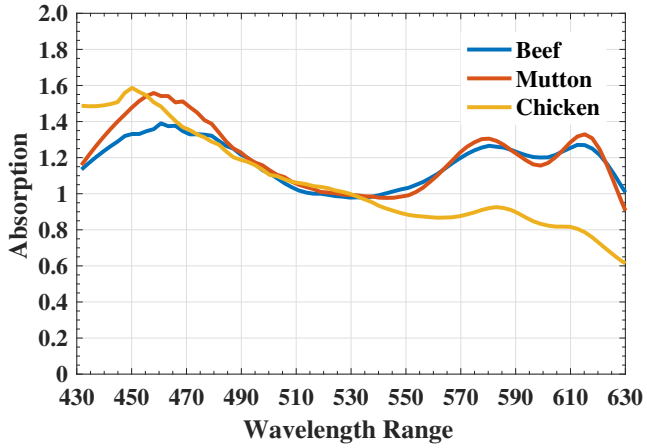

Figure 4. A single point Mb-based spectral features spectrum for each meat class. Soret absorption band (430-450 nm), meta-Mb (500–515 nm), dexa-Mb (545–560 nm), oxa-Mb (580–610 nm).

2.5. Classification

To classify the minced meat into Bovine, Ovine and Poultry, total samples were divided into training and test data with a ratio of 70% to 30%. In this study, non-linear SVM [49] has been used to classify the minced meat types.

SVM is a linear model; however, it has been widely used to classify both linear and non-linear problems [25]. The main idea of SVM is that it creates a hyperplane to divide the dataset into classes. For linearly separable data, it finds the maximal margin hyperplane between the classes. For non-linearly separable data, it maps the feature data into a high-dimensional space to find the optimal separating hyperplane [50]. In a nutshell, n training samples can be represented as (x_i, y_i) with $i = 1, 2, 3, \ldots, n$, where $x \, \epsilon \, R^k$ is k dimensional vector and $y_i \, \epsilon \, (1, -1)$ are the class labels. Furthermore, SVM uses a set of functions to take the input data and transform it into required form, known as kernels. Thus, the kernel function needs to be selected very carefully while training a SVM classifier.

In this study, radial basis function (RBF) kernel function is used for SVM. The values of the two main parameters of RBF are set as gamma = 0.8 and C= 1.0. The trained model was further validated through blind classification of the test data.

3. Results and Discussion

3.1. Spectral Features Analysis

The spectral information of samples, captured from HSI system, was distributed among 224 wavelength bands for this study. Figure 5 shows the 24 spectral bands of acquired samples, spanning over the 395–1000 nm range with the difference of 10 bands in each image. Figure 5a shows Ovine, Figure 5b shows Bovine and Figure 5c shows Poultry minced meat along with wavelength band number mentioned on all images.

However, the wavelength ranging from 400 to 430 nm has very low spectral intensities due to the limitation of halogen lamps; i.e., these lamps formed a very low-intensity response in the blue region, as shown in Figure 5d. Therefore, these bands needed to be removed before the classification process.

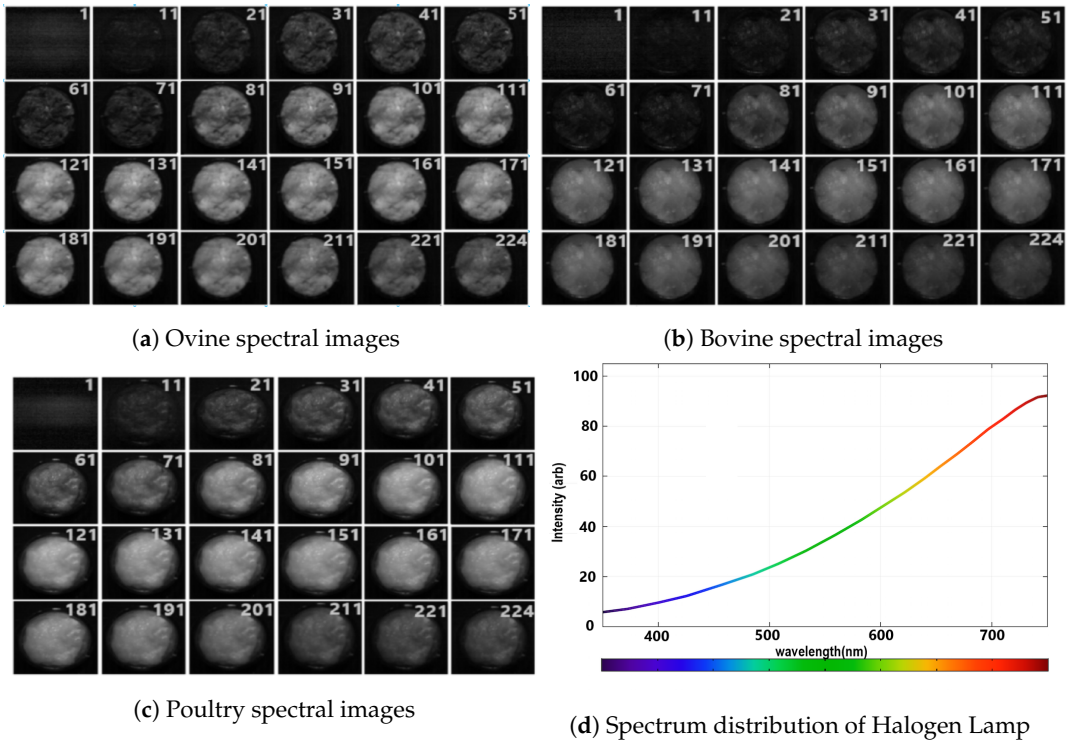

(**a**) Ovine spectral images

(**b**) Bovine spectral images

(**c**) Poultry spectral images

(**d**) Spectrum distribution of Halogen Lamp

Figure 5. The entire electromagnetic spectrum of minced meat type. (**a**) Ovine spectral images; (**b**) Bovine spectral images; (**c**) Poultry spectral images; (**d**) spectrum distribution of halogen lamp.

True-color image contains the information about samples similar to what is collected by the human visual system. The correlation coefficient is used widely to compute the true-color images for remote sensing data [45]. For this study the segmented regions (such as θ_R (Red), θ_G (green) and θ_B (blue)) have been examined for each band. The reflectance values are used to compute the correlation values. The highest value represents the most important wavelength in the segmented region; e.g., for Bovine minced meat, 492, 569 and 688 nm bands were selected based on the correlation values, as shown in Table 2.

Figure 6a shows the Mb spectral patterns of each minced meat which contains the Mb pigments at the range of 470–630 nm and oxidation levels at 760–1000 nm. The acquired spectrum contains random noises which affect the classification results; thus, Figure 6b–f shows the Golay filtering results for noise removal. It can be clearly seen that degree of polynomial and window size (n) must be selected appropriately to acquire the noise-free Mb pigments. Window size 7 and 9 smooths the spectral features like dexa-Mb and oxa-Mb, as shown in Figures 6d,e; however, the ambient noises are still visible in the range of 430–510 nm which contains the critical information of meta-Mb and soret absorption. Thus, these ambient noises are removed with the window size 11 for golay filtering. Figure 6f shows noise-free spectra and preserves the most important information regarding *Mb* pigments.

Table 2. The correlation values for true-color images. The underlined boldface values show the selected wavelengths (ñm) used to formulate true-color images

Band #	θ_B			Band #	θ_G			Band #	θ_R		
	Bovine	Ovine	Poultry		Bovine	Ovine	Poultry		Bovine	Ovine	Poultry
450 nm	0.690	**0.9710**	**0.969**	505 nm	0.933	0.959	0.959	607 nm	0.969	0.943	0.942
452 nm	0.700	0.969	0.967	508 nm	0.918	0.960	0.958	609 nm	0.996	0.942	0.941
455 nm	0.723	0.968	0.966	510 nm	0.916	**0.962**	0.960	612 nm	0.997	0.942	0.942
458 nm	0.757	0.967	0.966	513 nm	0.931	0.962	**0.961**	615 nm	0.997	0.943	0.942
460 nm	0.771	0.966	0.965	516 nm	0.940	0.959	0.957	617 nm	0.997	0.942	0.942
463 nm	0.790	0.967	0.966	518 nm	0.930	0.958	0.959	620 nm	0.998	0.942	0.941
465 nm	0.835	0.968	0.966	521 nm	0.927	0.960	0.958	623 nm	0.998	0.943	0.941
468 nm	0.858	0.969	0.965	524 nm	0.937	0.959	0.957	626 nm	0.997	0.944	0.942
471 nm	0.861	0.965	0.968	526 nm	0.942	0.957	0.955	628 nm	0.998	0.944	0.943
473 nm	0.885	0.966	0.964	529 nm	0.933	0.955	0.953	631 nm	0.998	0.944	0.943
476 nm	0.904	0.965	0.964	532 nm	0.928	0.955	0.953	634 nm	0.998	0.942	0.943
479 nm	0.907	0.964	0.962	534 nm	0.937	0.956	0.953	636 nm	0.998	0.942	0.942
481 nm	0.917	0.964	0.962	537 nm	0.939	0.953	0.951	639 nm	0.998	0.942	0.942
484 nm	0.925	0.963	0.961	540 nm	0.931	0.953	0.951	642 nm	0.998	0.945	0.944
487 nm	0.929	0.962	0.960	542 nm	0.927	0.953	0.951	644 nm	0.998	0.945	0.945
489 nm	0.925	0.962	0.961	545 nm	0.932	0.952	0.950	647 nm	0.998	0.945	0.945
492 nm	**0.933**	0.961	0.959	548 nm	0.934	0.950	0.948	650 nm	0.998	0.943	0.943
495 nm	0.929	0.958	0.957	550 nm	0.931	0.950	0.949	652 nm	0.998	0.942	0.942
497 nm	0.923	0.96	0.958	553 nm	0.935	0.952	0.950	655 nm	0.998	0.944	0.943
500 nm	0.931	0.962	0.960	556 nm	0.946	0.951	0.949	658 nm	0.998	0.945	0.944
				558 nm	0.952	0.950	0.948	661 nm	0.998	0.948	0.947
				561 nm	0.947	0.949	0.947	663 nm	0.998	**0.949**	0.948
				564 nm	0.945	0.951	0.949	666 nm	0.998	0.947	0.947
				566 nm	0.952	0.952	0.950	669 nm	0.9990	0.945	0.945
				569 nm	**0.959**	0.951	0.948	671 nm	0.9991	0.944	0.944
				572 nm	0.958	0.948	0.946	674 nm	0.9990	0.944	0.944
								677 nm	0.998	0.945	0.946
								680 nm	0.998	0.947	0.947
								682 nm	0.9990	0.948	**0.948**
								685 nm	0.9991	0.947	0.947
								688 nm	**0.9992**	0.946	0.946
								690 nm	0.9991	0.946	0.946
								693 nm	0.9991	0.945	0.946
								696 nm	0.9990	0.947	0.947

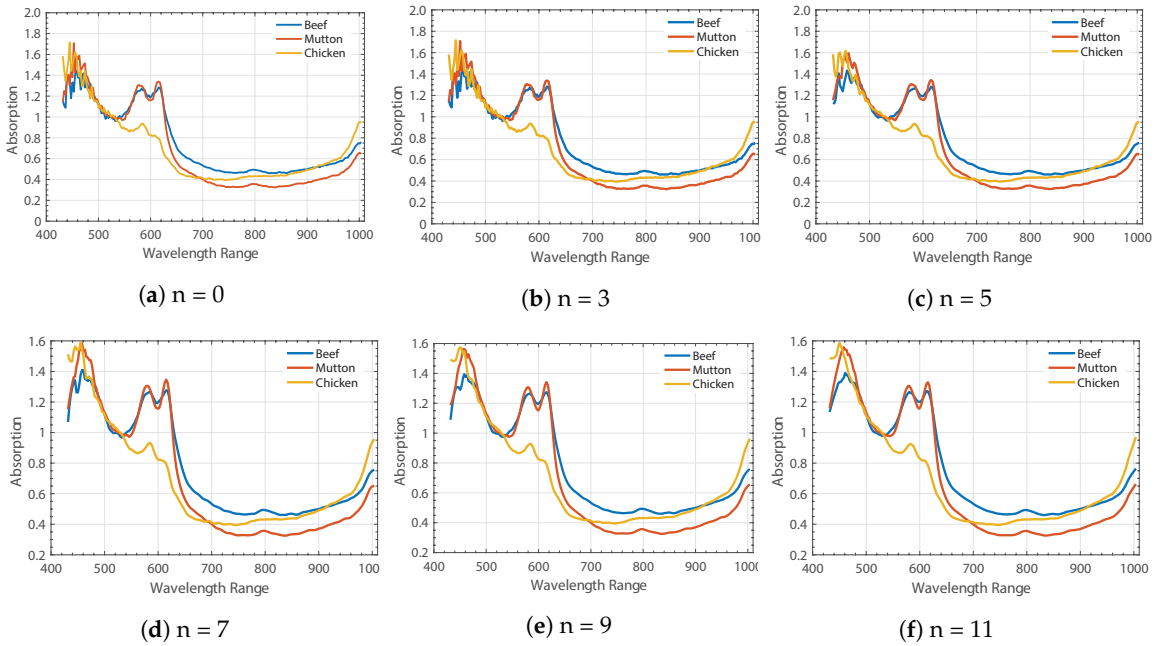

(**a**) n = 0 (**b**) n = 3 (**c**) n = 5

(**d**) n = 7 (**e**) n = 9 (**f**) n = 11

Figure 6. Savitzky–Golay spectral Pre-processing with several window sizes (n) for smooth Mb spectrum.

The mean spectral features extracted from Mb spectra through pre-processing and classical absorption spectrum for each minced meat are shown in Figures 7a–c. The Mb spectral feature difference within the intensity values from the classical absorption spectral methods can be observed in these images. The intensity spectrum variation for Bovine and Ovine meat classes is high due to the presence of high Mb values, whereas it is considerably lower in poultry minced meat. The combined spectra of each class indicates a clear difference in the range of the spectrum, as shown in Figure 6f.

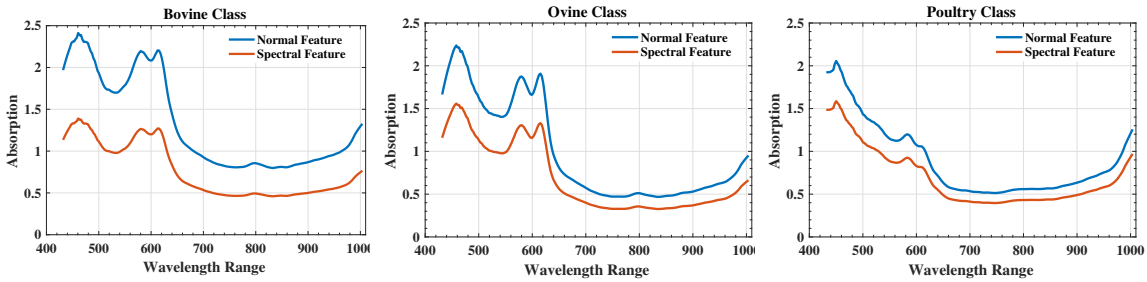

(**a**) Bovine spectrum (**b**) Ovine spectrum (**c**) Poultry spectrum

Figure 7. Difference in spectrum representations of Mb-based spectral features (spectral features) and classical absorption feature (normal Feature) of Bovine, Ovine and Poultry class minced meat.

3.2. Meat-Type Classification

For classification, non linear SVM was trained on $60 \times 50 \times 211 = 633,000$ features extracted from each sample category (Bovine, Ovine and Poultry). A total of 14 ROIs giving $(14 \times 633,000 = 8,862,000)$ features were randomly chosen from each minced meat class, which were further split into 70:30 ratio as training and testing data. To compute the classification average accuracy, the following method was adopted.

$$Accuracy = \frac{T.P}{T.S} \tag{6}$$

where $T.P$ and $T.S$ represent the true predictions and the total number of samples, respectively. Table 3 shows the training accuracy of the SVM classifier by using Mb based spectral features, with the average accuracy of 0.985.

Table 3. Confusion matrix of the training set.

Class	Ovine	Poultry	Bovine
Ovine	0.98	0	0.02
Poultry	0	0.994	0.006
Bovine	0.023	0	0.977
Average Accuracy: 98.5			

Finally, to validate the results, 11,394,000 features from 18 different minced meat samples were tested containing 6 samples from each meat type and achieved an overall accuracy of 0.888, as shown in Table 4. Figures 8–12 represent the pictorial classification results of our proposed spectral pattern, whereas Figure 9 represents the ground truth of the each mined meat. Figure 10 shows the classification results of Bovine minced meat, Figure 11 represents the Ovine minced meat and Figure 12 contains the poultry minced meat classification results. Furthermore, to make the predictions between Bovine and Ovine, a minimum of 70% for the threshold was considered to be optimal. The individual threshold values for each minced meat class can be observed in Table 5, where Bovine= class 1, Poultry = class 2 and Ovine = class 3. Sample 5 in Bovine and sample 3 in Ovine represent misclassifications.

Table 4. Confusion matrix of the test set.

Class	Ovine	Poultry	Bovine
Ovine	0.768	0.002	0.23
Poultry	0.001	0.997	0.002
Bovine	0.18	0.01	0.810
Average Accuracy: 88.8			

(**a**) Bovine minced Meat (**b**) Ovine minced Meat (**c**) Poultry minced meat

Figure 8. Color ROI representation of each minced meat type. (**a**) Bovine; (**b**) Ovine; (**c**) Poultry

(**a**) Bovine class (**b**) Ovine class (**c**) Poultry class

Figure 9. Ground truth representations for classification of minced meat types. (**a**) Bovine class; (**b**) Ovine class; and (**c**) Poultry class.

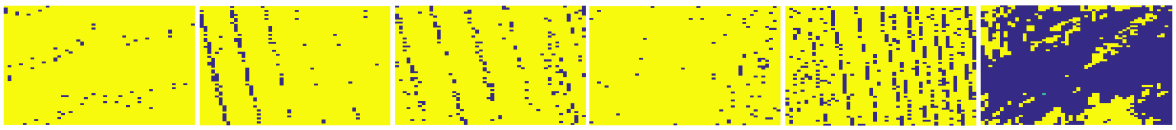

(**a**) Acc = 0.980 (**b**) Acc = 0.951 (**c**) Acc = 0.929 (**d**) Acc = 0.975 (**e**) Acc =0.833 (**f**) Acc = 0.209

Figure 10. Classification results for the Bovine minced meat class. Spots in Bovine minced meat class represent spectral misclassifications of Ovine minced meat class and Acc represents the accuracy of the Bovine class for each sample.

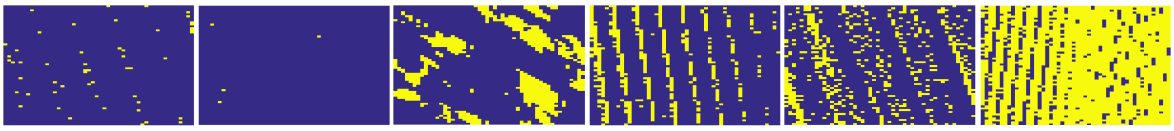

(**a**) Acc = 0.963 (**b**) Acc = 0.998 (**c**) Acc = 0.783 (**d**) Acc = 0.811 (**e**) Acc = 0.814 (**f**) Acc = 0.232

Figure 11. Classification results for the Ovine minced meat class. Spots in ovine minced meat class represent the spectral misclassifications of Bovine minced meat class and Acc represents the accuracy of the Ovine class for each sample.

(**a**) Acc = 1.00 (**b**) Acc = 1.00 (**c**) Acc = 1.00 (**d**) Acc = 1.00 (**e**) Acc = 0.9996 (**f**) Acc = 0.991

Figure 12. Classification results for the poultry minced meat class. Spots in poultry minced meat class represent the spectral misclassifications of Bovine and Ovine minced meat classes and Acc represents the accuracy of the poultry class for each sample.

Table 5. Bovine, Ovine and Poultry minced meat classification performance; class1, class2 and class3 represent Bovine, Poultry and Ovine, respectively.

Sample #	Bovine			Poultry			Ovine		
	Class 1	Class 2	Class 3	Class 1	Class 2	Class 3	Class 1	Class 2	Class 3
1	0.980	0.0	0.200	0.0	0.999	0.0	0.185	0.0	0.8143
2	0.9513	0.0	0.048	0.0	0.999	0.0	0.037	0.0	0.963
3	0.833	0.0	0.166	0.0	0.999	0.0	0.7680	0.0	0.232
4	0.929	0.0	0.070	0.0	0.999	0.0	0.0013	0.0	0.998
5	0.209	0.01	0.790	0.0003	0.9996	0.0	0.216	0.0	0.783
6	0.9753	0.0	0.024	0.0	0.991	0.009	0.188	0.0	0.811
Accuracy		81.01%			99.97%			76.88%	

3.3. Comparison With State-of-the-Art PCA Models

Table 6 presents the comparative results with state-of-the-art classical spectral pre-processing methods on minced meat test data. To ensure correct comparison, the hyper-parameters were optimized according to the proposed studies in the literature [25,32,51]. The classical pre-processing methods evaluate the response of test data through PCA, which in this study gave the overall accuracy of 82.01%. However, by utilizing the pipeline proposed by Ropodi et al. [25] the accuracy achieved was 94.00%. This proposed pipeline consists of two stages; at stage 1 the accuracy was 82.01%, whereas it increased to 94.00% in stage 2 due the correct classification of misclassified samples by increasing the train set using correctly classified samples. Moreover, the proposed pre-processing and Mb spectral features for the minced meat classification method outperformed several classical methods by achieving the overall accuracy of 88.88%.

Table 6. Comparative results with the state-of-the-art methods using same test data.

Feature	Classifier	Optimization	Accuracy
Reflectance Spectrum + PCA [32]	SMO	rbf ; Tolerance=0.001; C=1.0	82.01%
Reflectance Spectrum + PCA [25]	2-Step SVM	rbf ; Tolerance=0.001; C=1.0	94.00%
Reflectance + PCA + GLGCM [51]	SVM	rbf ;Tolerance=0.001; C=1.0	72.22%
Proposed Methodology			
Spectral Features	SVM	rbf ; Tolerance=0.001; C=1.0	88.88%

4. Conclusions

This study formulates true-color images to extract accurate ROIs similar those from human perception. This study also proposed a novel *isos-bestic* based Mb spectral features extraction for minced meat (Bovine, Ovine and Poultry) using an HSI-system. The extracted features describe the formation of proteins pigments, i.e., the chemical composition of meat respiratory pigments. These extracted features are later fed to a nonlinear SVM classifier for the classification of minced meat. The experimental results reveal that the proposed pipeline significantly improves the performance as compared to the state-of-the-art methods. The classical methods use spectral features such as reflectance and absorption to classify the *chunk* meat types, whereas in this study, we used *isos-bestic*-based Mb spectral features for minced meat-type classification with an average accuracy of 88.88%. The future direction of our study is to analyze the classification accuracy based on several deep architectures, such as AlexNet, ResNet, DesNet and GoogleNet.

Author Contributions: Conceptualization, H.A., M.A. (Muhammad Ahmad), A.S., M.N.Y., M.A. (Mohsin Ali) and M.H.K.; data curation, H.A., M.A. (Muhammad Ahmad) and Z.S.; formal analysis, H.A.; investigation, H.A. and M.A. (Muhammad Ahmad); methodology, H.A., M.A. (Muhammad Ahmad), A.S. and M.A.Z.; supervision, M.A. (Muhammad Ahmad) and A.S.; validation, H.A., M.A. (Muhammad Ahmad), M.N.Y. and Z.S.; visualization, H.A., M.A. (Muhammad Ahmad), M.N.Y., M.A. (Mohsin Ali), M.H.K. and Z.S.; writing—original draft, H.A., M.A. (Muhammad Ahmad), M.A.Z., M.H.K. and Z.S.; writing—review and editing, H.A., M.A. (Muhammad Ahmad),

A.S., M.N.Y., M.A.Z., M.A. (Mohsin Ali), M.H.K. and Z.S. All authors have read and agreed to the published version of the manuscript.

Funding: "This research received no external funding"

Conflicts of Interest: "The authors declare no conflict of interest."

Declaration of Competing Interest: KFUEIT plans to file a patent based on this work, in which H. Ayaz, M. Ahmad and A. Sohaib are inventors.

References

1. The Color of Meat and Poultry. Available online: https://www.fsis.usda.gov/wps/portal/fsis/topics/food-safety-education/get-answers/food-safety-fact-sheets/meat-preparation/the-color-of-meat-and-poultry/the-color-of-meat-and-poultry/ct_index#:~:text=When%20meat%20is%20fresh%20and,a%20pleasingly%20cherry%2Dred%20color. (accessed on 19 August 2020).
2. American Meat Science Association; *AMSA Meat Color Measurement Guidelines: AMSA*; American Meat Science Association: Savoy, IL, USA, 2012.
3. Tang, J.; Faustman, C.; Hoagland, T. Krzywicki revisited: Equations for spectrophotometric determination of myoglobin redox forms in aqueous meat extracts. *J. Food Sci.* **2004**, *69*, C717–C720. [CrossRef]
4. Viriyarattanasak, C.; Hamada-Sato, N.; Watanabe, M.; Kajiwara, K.; Suzuki, T. Equations for spectrophotometric determination of relative concentrations of myoglobin derivatives in aqueous tuna meat extracts. *Food Chem.* **2011**, *127*, 656–661. [CrossRef]
5. Cheng, L.; Liu, G.; He, J.; Wan, G.; Ma, C.; Ban, J.; Ma, L. Non-destructive assessment of the myoglobin content of Tan sheep using hyperspectral imaging. *Meat Sci.* **2019**, *167*, 107988. [CrossRef] [PubMed]
6. Wu, S.; Luo, X.; Yang, X.; Hopkins, D.L.; Mao, Y.; Zhang, Y. Understanding the development of color and color stability of dark cutting beef based on mitochondrial proteomics. *Meat Sci.* **2020**, *163*, 108046. [CrossRef] [PubMed]
7. Ballin, N.Z. Authentication of meat and meat products. *Meat Sci.* **2010**, *86*, 577–587. [CrossRef] [PubMed]
8. Stanciu, S.; Stanciuc, N.; Dumitrascu, L.; Ion, R.; Nistor, C. The effects of horse meat scandal on Romanian meat market. *SEA-Pract. Appl. Sci.* **2013**, *1*, 174–181.
9. Cawthorn, D.M.; Steinman, H.A.; Hoffman, L.C. A high incidence of species substitution and mislabelling detected in meat products sold in South Africa. *Food Control* **2013**, *32*, 440–449. [CrossRef]
10. Bottero, M.T.; Dalmasso, A. Animal species identification in food products: Evolution of biomolecular methods. *Vet. J.* **2011**, *190*, 34–38. [CrossRef]
11. Zhu, H.; Yang, X.; Zhang, C.; Zhu, C.; Tao, G.; Zhao, L.; Tang, S.; Shu, Z.; Cai, J.; Dai, S.; et al. Red and processed meat intake is associated with higher gastric cancer risk: a meta-analysis of epidemiological observational studies. *PLoS ONE* **2013**, *8*, e70955. [CrossRef]
12. Barnard, N.; Levin, S.; Trapp, C. Meat consumption as a risk factor for type 2 diabetes. *Nutrients* **2014**, *6*, 897–910. [CrossRef]
13. Sinha, R.; Cross, A.J.; Graubard, B.I.; Leitzmann, M.F.; Schatzkin, A. Meat intake and mortality: A prospective study of over half a million people. *Arch. Internal Med.* **2009**, *169*, 562–571. [CrossRef] [PubMed]
14. Kamruzzaman, M.; Makino, Y.; Oshita, S.; Liu, S. Assessment of visible near-infrared hyperspectral imaging as a tool for detection of horsemeat adulteration in minced beef. *Food Bioprocess Technol.* **2015**, *8*, 1054–1062. [CrossRef]
15. Ahmed, M.U.; Hasan, Q.; Hossain, M.M.; Saito, M.; Tamiya, E. Meat species identification based on the loop mediated isothermal amplification and electrochemical DNA sensor. *Food Control* **2010**, *21*, 599–605. [CrossRef]
16. Vallejo-Cordoba, B.; González-Córdova, A.F.; Mazorra-Manzano, M.A.; Rodríguez-Ramírez, R. Caillary electrophoresis for the analysis of meat authenticity. *J. Sep. Sci.* **2005**, *28*, 826–836. [CrossRef] [PubMed]
17. ElMasry, G.; Barbin, D.F.; Sun, D.W.; Allen, P. Meat quality evaluation by hyperspectral imaging technique: an overview. *Crit. Rev. Food Sci. Nutr.* **2012**, *52*, 689–711. [CrossRef] [PubMed]
18. Kamruzzaman, M.; ElMasry, G.; Sun, D.W.; Allen, P. Application of NIR hyperspectral imaging for discrimination of lamb muscles. *J. Food Eng.* **2011**, *104*, 332–340. [CrossRef]
19. Ma, J.; Sun, D.W.; Pu, H.; Cheng, J.H.; Wei, Q. Advanced techniques for hyperspectral imaging in the food industry: Principles and recent applications. *Ann. Rev. Food Sci. Technol.* **2019**, *10*, 197–220. [CrossRef]

20. Suman, S.P.; Joseph, P. Myoglobin chemistry and meat color. *Ann. Rev. Food Sci. Technol.* **2013**, *4*, 79–99. [CrossRef]
21. Denoyelle, C.; Berny, F. Objective measurement of veal color for classification purposes. *Meat Sci.* **1999**, *53*, 203–209. [CrossRef]
22. Fletcher, D. Broiler breast meat color variation, pH, and texture. *Poult. Sci.* **1999**, *78*, 1323–1327. [CrossRef]
23. Xing, J.; Ngadi, M.; Gunenc, A.; Prasher, S.; Gariepy, C. Use of visible spectroscopy for quality classification of intact pork meat. *J. Food Eng.* **2007**, *82*, 135–141. [CrossRef]
24. Liu, Y.; Chen, Y.R. Analysis of visible reflectance spectra of stored, cooked and diseased chicken meats. *Meat Sci.* **2001**, *58*, 395–401. [CrossRef]
25. Ropodi, A.I.; Panagou, E.Z.; Nychas, G.J.E. Multispectral imaging (MSI): A promising method for the detection of minced beef adulteration with horsemeat. *Food Control* **2017**, *73*, 57–63. [CrossRef]
26. Ahmad, M.; Khan, A.; Khan, A.M.; Mazzara, M.; Distefano, S.; Sohaib, A.; Nibouche, O. Spatial prior fuzziness pool-based interactive classification of hyperspectral images. *Remote Sens.* **2019**, *11*, 1136. [CrossRef]
27. Ahmad, M.; Shabbir, S.; Oliva, D.; Mazzara, M.; Distefano, S. Spatial-prior Generalized Fuzziness Extreme Learning Machine Autoencoder-based Active Learning for Hyperspectral Image Classification. *Optik-Int. J. Light Electron Opt.* **2020**. [CrossRef]
28. Ahmad, M.; Raza, R.A.; Mazzara, M. Multiclass Non-Randomized Spectral–Spatial Active Learning for Hyperspectral Image Classification. *Appl. Sci.* **2020**, *10*, 4739. [CrossRef]
29. Fu, X.; Chen, J. A review of hyperspectral imaging for chicken meat safety and quality evaluation: application, hardware, and software. *Compr. Rev. Food Sci. Food Saf.* **2019**, *18*, 535–547. [CrossRef]
30. Fowler, S.M.; Schmidt, H.; Scheier, R.; Hopkins, D.L. Raman spectroscopy for predicting meat quality traits. In *Advanced Technologies for Meat Processing*; CRC Press: Cleveland, OH, USA, 2017; pp. 83–112.
31. Velásquez, L.; Cruz-Tirado, J.; Siche, R.; Quevedo, R. An application based on the decision tree to classify the marbling of beef by hyperspectral imaging. *Meat Sci.* **2017**, *133*, 43–50. [CrossRef] [PubMed]
32. Sanz, J.A.; Fernandes, A.M.; Barrenechea, E.; Silva, S.; Santos, V.; Gonçalves, N.; Paternain, D.; Jurio, A.; Melo-Pinto, P. Lamb muscle discrimination using hyperspectral imaging: Comparison of various machine learning algorithms. *J. Food Eng.* **2016**, *174*, 92–100. [CrossRef]
33. Al-Sarayreh, M.; M Reis, M.; Qi Yan, W.; Klette, R. Detection of red-meat adulteration by deep spectral–spatial features in hyperspectral images. *J. Imaging* **2018**, *4*, 63. [CrossRef]
34. Qiao, J.; Ngadi, M.O.; Wang, N.; Gariépy, C.; Prasher, S.O. Pork quality and marbling level assessment using a hyperspectral imaging system. *J. Food Eng.* **2007**, *83*, 10–16. [CrossRef]
35. Qiao, J.; Wang, N.; Ngadi, M.; Gunenc, A.; Monroy, M.; Gariepy, C.; Prasher, S. Prediction of drip-loss, pH, and color for pork using a hyperspectral imaging technique. *Meat Sci.* **2007**, *76*, 1–8. [CrossRef] [PubMed]
36. ElMasry, G.; Sun, D.W.; Allen, P. Near-infrared hyperspectral imaging for predicting colour, pH and tenderness of fresh beef. *J. Food Eng.* **2012**, *110*, 127–140. [CrossRef]
37. Barbon, S.; Costa Barbon, A.P.A.d.; Mantovani, R.G.; Barbin, D.F. Machine Learning Applied to Near-Infrared Spectra for Chicken Meat Classification. *J. Spectrosc.* **2018**, *2018*, 12. [CrossRef]
38. Zhang, Y.; Jiang, H.; Wang, W. Feasibility of the detection of carrageenan adulteration in chicken meat using visible/near-infrared (vis/nir) hyperspectral imaging. *Appl. Sci.* **2019**, *9*, 3926. [CrossRef]
39. Rady, A.; Adedeji, A.A. Application of Hyperspectral Imaging and Machine Learning Methods to Detect and Quantify Adulterants in Minced Meats. *Food Anal. Methods* **2020**, 1–12. [CrossRef]
40. Khan, M.H.; Saleem, Z.; Ahmad, M.; Sohaib, A.; Ayaz, H. Unsupervised adulterated red-chili pepper content transformation for hyperspectral classification. *arXiv* **2019**, arXiv:1911.03711.
41. Farrand, W.H.; Singer, R.B.; Merényi, E. Retrieval of apparent surface reflectance from AVIRIS data: A comparison of empirical line, radiative transfer, and spectral mixture methods. *Remote Sens. Environ.* **1994**, *47*, 311–321. [CrossRef]
42. Reis, M.M.; Van Beers, R.; Al-Sarayreh, M.; Shorten, P.; Yan, W.Q.; Saeys, W.; Klette, R.; Craigie, C. Chemometrics and hyperspectral imaging applied to assessment of chemical, textural and structural characteristics of meat. *Meat Sci.* **2018**, *144*, 100–109. [CrossRef]
43. Mamani-Linares, L.; Gallo, C.; Alomar, D. Identification of cattle, llama and horse meat by near infrared reflectance or transflectance spectroscopy. *Meat Sci.* **2012**, *90*, 378–385. [CrossRef]

44. Cozzolino, D.; Murray, I. Identification of animal meat muscles by visible and near infrared reflectance spectroscopy. *LWT-Food Sci. Technol.* **2004**, *37*, 447–452. [CrossRef]
45. Su, H.; Du, Q.; Du, P. Hyperspectral image visualization using band selection. *IEEE J. Sel. Top. Appl. Earth Obs. Remote Sens.* **2013**, *7*, 2647–2658. [CrossRef]
46. Nelson-Wong, E.; Howarth, S.; Winter, D.A.; Callaghan, J.P. Application of autocorrelation and cross-correlation analyses in human movement and rehabilitation research. *J. Orthop. Sports Phys. Therapy* **2009**, *39*, 287–295. [CrossRef]
47. Yu, Y.; Yu, H.; Guo, L.; Li, J.; Chu, Y.; Tang, Y.; Tang, S.; Wang, F. Accuracy and stability improvement in detecting Wuchang rice adulteration by piece-wise multiplicative scatter correction in the hyperspectral imaging system. *Anal. Methods* **2018**, *10*, 3224–3231. [CrossRef]
48. Schafer, R.W.; others. What is a Savitzky-Golay filter. *IEEE Signal Process. Mag.* **2011**, *28*, 111–117. [CrossRef]
49. Schölkopf, B.; Burges, C.J.; Smola, A.J.; others. *Advances in Kernel Methods: Support Vector Learning*; MIT Press: Cambridge, MA, USA, 1999.
50. Chen, K.; Sun, X.; Qin, C.; Tang, X. Color grading of beef fat by using computer vision and support vector machine. *Comput. Electron. Agric.* **2010**, *70*, 27–32. [CrossRef]
51. Xiong, Z.; Sun, D.W.; Pu, H.; Zhu, Z.; Luo, M. Combination of spectra and texture data of hyperspectral imaging for differentiating between free-range and broiler chicken meats. *LWT-Food Sci. Technol.* **2015**, *60*, 649–655. [CrossRef]